Arch. Metall. Mater. **69** (2024), 3, 955-963

DOI: https://doi.org/10.24425/amm.2024.150915

M.A. BOUCHELARM[1*], M. CHAFI[1], A. BOULENOUAR[1], N. BENSEDDIQ[2]

EFFECT OF THE MATERIAL GRADATION ON THE FRACTURE TRAJECTORY IN CERAMIC/METAL FUNCTIONALLY GRADED MATERIALS

This paper is based on a 2D numerical study of crack initiation and growth in ceramic/metal functionally graded materials (FGMs) under mixed mode condition. The finite element method is used for modeling the crack growth trajectory. Two types of ceramic/metal FGMs are considered to explore the effect of the material gradation on the fracture trajectory. The variation of the material properties is declared in a program by defining the material parameters at the center of the elements. After a numerical evaluation of the fracture parameters, the Maximum Tangential Stress (MTS) criterion is used for the prediction of crack propagation direction with respect to the crack axis. The difference in the crack growth trajectory can be related to the influence of the material gradient. In addition, it was found that the easiest way for the crack propagation is when the crack is perpendicular to the material gradation. A crack located on the rigid side of the specimen deviates less compared to the one on the soft side.

Keywords: Mixed mode loading; functionally graded materials; Stress intensity factors; T-stress; Crack propagation; ceramic/metal FGM

1. Introduction

Functionally graded materials (FGM) are a new material concept of sophisticated composites, designed with a gradual variation of mechanical properties, microstructure and composition different from classic composites or homogeneous materials. This new generation of materials have a reputation of being ideal for the applications requiring various performances like the reduction of thermal stresses associated with the good mechanical properties by designing a ceramic/metal FGM. Because of the complex design of the FGMs, the study of fracture and crack propagation is very challenging.

Compared to the detailed studies on mode I fracture of FGMs, a limited number of works have been reported for the case of mixed mode fracture. Mixed-mode experimental and numerical study was carried out by Oral et al. [1] on fracture initial direction in FGMs. 2D dynamic mixed mode crack growth simulations was done on FGMs by Zhang and Paulino [2] by the mean of cohesive zone models. Using the extended finite element method (XFEM), Dimitri et al. [3] have been able to predict the crack direction for different loading conditions and to evaluate stress intensity factors (SIFs). The same approach (XFEM) was applied by Dolbow and Gosz [4] who considered an arbitrarily oriented crack in the plane problem. Kirugulige and Tippur [5] carried out dynamic fracture tests to investigate the crack growth in glass-filled epoxy FGM. Jin and Batra [6], Gu and Asaro [7] came up with quasi-static SIFs for cracks in FGM for distinct geometries and loading conditions.

It is known that the determination of the crack propagation trajectory is based on the determination of the SIFs, for that reason, accurate values of SIFs are necessary to predict the crack growth at each step. Various methods have been reported in the literature to accurately evaluate SIF for different materials [8-13]. Among several studies dealing with FGMs, Kim and Paulino [14] attempted to evaluate the crack propagation trajectory for FGMs through numerical simulations in the case of mixed-mode and non-proportional loading; they used a modified crack closure method. The same authors [15] carried out fracture analysis of nonhomogeneous orthotropic materials using a mixed mode J-integral formulation. In another study [16], SIFs were evaluated by the mean of the interaction integral method. Topal and Dag [17] performed a thermal fracture analysis of orthotropic FGMs using an equivalent domain integral approach. The displacement extrapolation technique was used by several authors to determine the stress intensity factors [18-20]. SIFs were determined by Rao and Rahman [21] using the element-free Galerkin

[1] DJILLALI LIABES UNIVERSITY OF SIDI BEL-ABBES- 22000- SIDI BEL-ABBES. LABORATOIRE DE MATÉRIAUX ET SYSTÈMES RÉACTIFS- LMSR, ALGERIA
[2] UNIVERSITY OF LILLE, UNITÉ DE MÉCANIQUE DE LILLE, EA 7512 UML 59000 LILLE, FRANCE

* Corresponding author: m.bouchelarm@yahoo.com

method for 2D arbitrary geometry FGMs. Using a generalized method, Chandran and Barsoum [22] determined K_I and K_{II} for center-cracked specimen. Dorduncu et al. [23] used peridynamic approach for modeling of two dimensional functionally graded plates. Dewei He et al. [24] carried out a study of fracture in functionally graded materials under thermal shock loading using peridynamics. Nguyen et al. [25] investigated the effect of porosities on crack propagation in FGM structures using the phase-field model. It was found that this method can accurately model the failure of porous structures.

Much of the literature focused on theoretical and numerical studies, there are relatively few experimental works dealing with the mixed mode fracture of functionally graded materials. Rousseau and Tippur [26] performed experimental four-point bending tests and investigated the fracture trajectory in epoxy/glass FGM beam. Experimental study was done by Tilbrook et al. [27] by the mean of fatigue and fracture tests of FGMs; they studied the influence of graded properties on their results. Xin Jin et al. [28] investigated the fracture in ZrO2/NiCr FGM under mixed mode condition. Abanto-Bueno and Lambros [29] experimentally studied the fracture behavior of a polymer-based functionally graded material. Digital image correlation technique was used to extract fracture parameters SIFs and T-stress [30].

The aim focus of this work is to numerically investigate the influence of the direction of material gradient on the mixed-mode fracture path in ceramic/metal FGMs. To this end, we have considered two types of FGMs, with different material gradients. A special algorithm has been developed by the mean of Ansys APDL, incorporating the material properties and a local fracture mechanics criterion to predict the crack growth path of FGM beam under three point bending. The mixed mode conditions are obtained by shifting the applied loading position with respect to crack axis.

2. Theoretical formulations

2.1. Determination of the SIFs

In this study, the displacement correlation technique DCT [31] is used to compute the mixed mode SIFs K_I and K_{II} for functionally graded materials. This correlation is performed on specific points located on the crack lips, the parameters K_I and K_{II} are respectively the mode I and mode II SIFs and are given by the following equations:

$$K_I = \frac{\mu_{tip}}{k_{tip}+1}\sqrt{\frac{2\pi}{L}}\left[4\left(v_b - v_d\right) - \left(v_c - v_e\right)\right] \tag{1}$$

$$K_{II} = \frac{\mu_{tip}}{k_{tip}+1}\sqrt{\frac{2\pi}{L}}\left[4\left(u_b - u_d\right) - \left(u_c - u_e\right)\right] \tag{2}$$

E_{tip}, υ_{tip} et μ_{tip} represent respectively, the elastic modulus, Poisson's ratio and shear modulus. These parameters are evaluated at the crack tip.

In linear elasticity, the parameter k_{tip} is equal to $\left(\frac{3-\nu_{tip}}{1+\nu_{tip}}\right)$ for plane stress and equal to $(3 - 4\nu_{tip})$ for plane strain.

L corresponds to the length of the element side connected to the crack front. u and v are, respectively, the displacements along the x and y directions.

It should be mentioned that for an improved calculation accuracy of the field in the vicinity crack front, a special quarter point finite element is considered. The middle side node of the element in the crack front is shifted to quarter length of the element

2.2. Determination of T-stress

The in-plane linear elastic stresses in the region of the crack tip can be defined as symmetric and antisymmetric fields, respectively known as mode I and mode II. The stress fields can be represented as an eigen series expansion [32-34]. Arround the crack front, where the higher order terms $O(r^{1/2})$ can be neglected, the mode I stress fields are:

$$\sigma_{xx} = \frac{K_{\mathrm{I}}}{\sqrt{2\pi r}}\cos\frac{1}{2}\theta\left[1-\sin\frac{1}{2}\theta\sin\frac{1}{2}\left(3\theta\right)\right] + T + O\left(r^{1/2}\right) \tag{3}$$

$$\sigma_{yy} = \frac{K_{\mathrm{I}}}{\sqrt{2\pi r}}\cos\frac{1}{2}\theta\left[1+\sin\frac{1}{2}\theta\sin\frac{1}{2}\left(3\theta\right)\right] + O\left(r^{1/2}\right) \tag{4}$$

$$\tau_{xy} = \frac{K_{\mathrm{I}}}{\sqrt{2\pi r}}\cos\frac{1}{2}\theta\sin\frac{1}{2}\theta\cos\frac{1}{2}\left(3\theta\right) + O\left(r^{1/2}\right) \tag{5}$$

And for mode II:

$$\sigma_{xx} = \frac{K_{\mathrm{II}}}{\sqrt{2\pi r}}\sin\frac{1}{2}\theta\left[2+\cos\frac{1}{2}\theta\cos\frac{1}{2}\left(3\theta\right)\right] + O\left(r^{1/2}\right) \tag{6}$$

$$\sigma_{yy} = \frac{K_{\mathrm{II}}}{\sqrt{2\pi r}}\sin\frac{1}{2}\theta\cos\frac{1}{2}\theta\cos\frac{1}{2}\left(3\theta\right) + O\left(r^{1/2}\right) \tag{7}$$

$$\tau_{xy} = \frac{K_{\mathrm{II}}}{\sqrt{2\pi r}}\cos\frac{1}{2}\theta\left[1-\sin\frac{1}{2}\theta\sin\frac{1}{2}\left(3\theta\right)\right] + O\left(r^{1/2}\right) \tag{8}$$

where σ_{xx}, σ_{yy} and τ_{xy} are the mode I stresses, r, θ, x and y are coordinates in conventional polar and Cartesian systems with the crack tip at the origin. The T term is a constant stress parallel to the crack namely the T-stress.

For a mixed mode loading, a singular term corresponding to mode I, or mode II or mixed (I+II) are considered. The methods used for mode I are therefore not valid for the case of a mixed mode I/II. T-stress can be determined without the use of SIFs

when both symmetric and antisymmetric properties of modes I and II are used. The stresses in the first half of the cracked specimen can be added to the stresses of the second half. The mode II stresses are simplified and the mode I stresses are doubled. This gives the possibility to determine T-stress by the following equations using finite element analysis [35].

$$T = \left(\sigma_{xx} - \sigma_{yy}\right)_{\theta=0} \tag{9}$$

$$T = \frac{1}{2}\left[\left(\sigma_{xx}\right)_{\theta=-\pi} + \left(\sigma_{xx}\right)_{\theta=\pi}\right] \tag{10}$$

$$T = \frac{1}{2}\left[\begin{array}{l}\left(\sigma_{xx} - \frac{1}{3}\left(\sigma_{yy}\right)\right)_{\theta=-(\pi/3)} + \\ + \left(\sigma_{xx} - \frac{1}{3}\left(\sigma_{yy}\right)\right)_{\theta=\pi/3}\end{array}\right] \tag{11}$$

$$T = \frac{1}{2}\left[\begin{array}{l}\left(\sigma_{xx} - \frac{1}{3}\left(\sigma_{yy}\right)\right)_{\theta=-(\pi/2)} + \\ + \left(\sigma_{xx} - \frac{1}{3}\left(\sigma_{yy}\right)\right)_{\theta=\pi/2}\end{array}\right] \tag{12}$$

$$T = \frac{1}{2}\left[\left(\sigma_{xx} - \sigma_{yy}\right)_{\theta=-(2\pi/3)} + \left(\sigma_{xx} - \left(\sigma_{yy}\right)_{\theta=2\pi/3}\right]\right. \tag{13}$$

It is convenient to use Eq. (10) since only one stress component is used.

A more efficient way to determine T-stress without using a very refined mesh is to use the displacement method. Hooke's law for small deformations can be written as follows:

$$\sigma_{xx} = E'\varepsilon_{xx} = E'\frac{du_x}{dx} \tag{14}$$

where: ε_{xx} et u_{xx} re the strain and displacement respectively parallel-to-the-crack and E' is defined as $E' = E$ for plane stress and $E' = \dfrac{E}{1-\nu^2}$ for plane strain. E is Young's modulus and ν is Poisson's ratio.

Using Eq. (14) for the upper and the lower crack lips, and summing the results, T-stress can be determined by:

$$T = \frac{1}{2}E'\left(\left(\frac{\mathrm{d}u_x}{\mathrm{d}x}\right)_{\theta=-\pi} + \left(\frac{\mathrm{d}u_x}{\mathrm{d}x}\right)_{\theta=\pi}\right) \tag{15}$$

Based on the displacements alone, T-stress is obtained using:

$$T = \frac{1}{2x}E'\left[u_x\left(x,-\pi\right) + u_x\left(x,\pi\right)\right] \tag{16}$$

2.3. Determination of the fracture trajectory

After a numerical evaluation of the SIFs, the fracture criterion must determine the crack propagation direction with respect to the crack axis. The fracture phenomenon is assumed to be driven by the circumferential stress intensity in the vicinity of the crack front. Introduced by Erdogan and Sih [36], the Maximum Tangential Stress (MTS) is a local criterion, based on the knowledge of the stress field at the crack tip. According to this criterion, the bifurcation initiates at the crack tip in the direction for which the circumferential stress $\sigma_{\theta\theta}$ is maximum.

In linear elasticity, it is translated to:

$$\sigma_{\theta\theta} > 0,\ \frac{\partial\sigma_{\theta\theta}}{\partial\theta} = 0\ \ et\ \frac{\partial^2\sigma_{\theta\theta}}{\partial\theta^2} < 0 \tag{17}$$

$$\sigma_{\theta\theta} = \frac{1}{4\sqrt{2\pi}}\left[\begin{array}{l}K_I\left(\cos\frac{\theta}{2} + \cos\frac{3\theta}{2}\right) - \\ 3K_{II}\left(\sin\frac{\theta}{2} + \sin\frac{3\theta}{2}\right)\end{array}\right] \tag{18}$$

One can deduce:

$$K_I\cos\theta + K_{II}\left(3\cos\theta - 1\right) = 0 \tag{19}$$

The crack direction can be expressed as follows :

$$\mathrm{tg}\left(\frac{\theta}{2}\right) = \frac{1}{4}\frac{K_I}{K_{II}} \pm \frac{1}{4}\sqrt{\left(\frac{K_I}{K_{II}}\right)^2 + 8} \tag{20}$$

$$\theta = 2\ \mathrm{arctg}\left[\frac{1}{4}\frac{K_I}{K_{II}} \pm \frac{1}{4}\sqrt{\left(\frac{K_I}{K_{II}}\right)^2 + 8}\right] \tag{21}$$

For this criterion, the propagation direction θ_0 is independent of the nature of the material, especially the Poisson's ratio v. This criterion needs quite-few remeshing for every step of crack growth. It is also possible to use it for materials with elastic-plastic behavior for the case of confined plastic zone [37].

3. Crack growth modeling

The fracture initial angle θ at each propagation increment Δa is determined by solving the equations system defining the chosen criterion. In this study, we use the MTS criterion. The propagation angle θ is calculated in the local reference system with respect to the crack axis. For the proposed examples, the calculations are performed step by step, assuming small crack propagations Δa. To explain how the program works for the crack propagation, a flowchart is presented in Fig. 1. In each step, SIFs K_I and K_{II} are calculated first using the displacement field information in the vicinity of the crack. After finding the propagation angle θ using the fracture criterion, we assume a small crack extension Δa in the calculated direction. Then in the next step, the crack front is automatically shifted to extend the crack. The new stress intensity factors K_I and K_{II} are calculated to determine the new propagation angle. It is noted that an advancing front method is used to generate the FE mesh, where the mesh generation and the singular elements construction are incorporated in the program, simplifying the analysis of the crack growth. The algorithm can be repeated continuously to the ultimate failure of the specimen or can be stopped by the user.

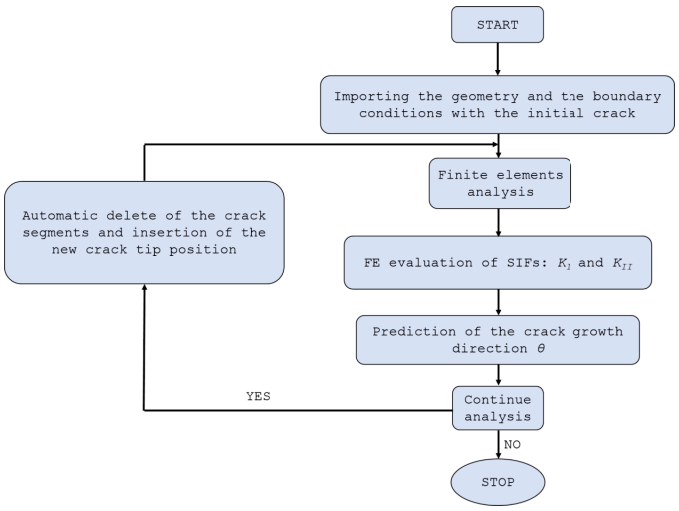

Fig. 1. Flowchart of the crack modeling algorithm

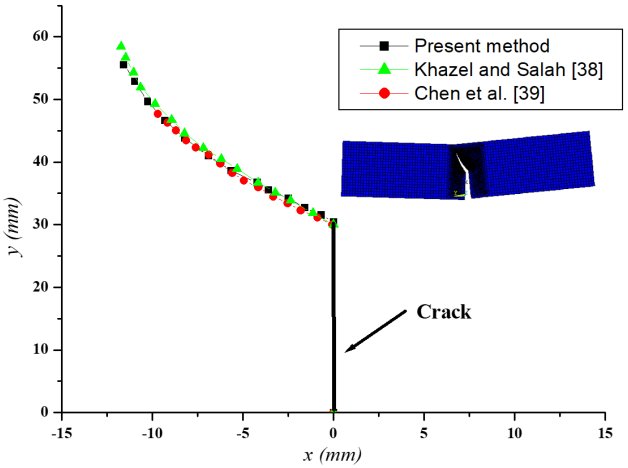

Fig. 3. Comparison of crack path trajectories for FGM beam

4. Finite element analysis

4.1. Numerical validation

In this section, fracture simulations for FGM material were carried out in order to validate the proposed numerical method. Cracked FGM beam subjected to three-point bending was considered. Fig. 2 shows the FGM beam geometry and boundary conditions considering an offset loading. A linear variation of the material properties is chosen according to the proposed examples of Khazal [38] and Chen [39]. FE modelling was conducted using ANSYS APDL. The structure was modeled in 2D under plane strain conditions using isoparametric quadrilateral Plane 82 elements, which have eight nodes. A total number of 2394 elements is used, and special singular elements mesh is investigated at the crack-tip to consider the singularity of stress and deformations fields.

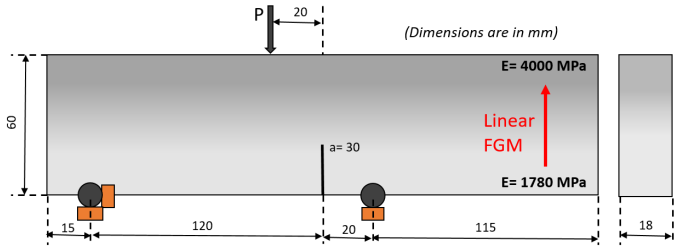

Fig. 2. Cracked FGM beam subjected to three-point bending [38-39]

In Fig. 3, the crack path trajectory obtained by the proposed method is compared to the numerical results of Khazal [38] using the extended element free Galerkin method, and to the crack trajectory using the scaled boundary finite element method proposed by Chen [39]. Clearly, we have accurate results and a good agreement is obtained between the predicted crack trajectories by the numerical methods cited above. One can conclude that the developed approach of the current study is successfully validated and can be used for the next investigations.

4.2. Effect of the material gradation

To study the effect of the material gradation on the crack growth in ceramic/metal FGMs subjected to mixed-mode loading, we considered two sorts of functionally graded materials: FGM-A corresponds to a material which the gradation is along the y-axis (Fig. 4a), and FGM-B whose material gradation is along the x-axis (Fig. 4b). For both materials, the specimen is loaded by an applied force located in one of the three positions A, B or C according to the configurations shown in Fig. 4.

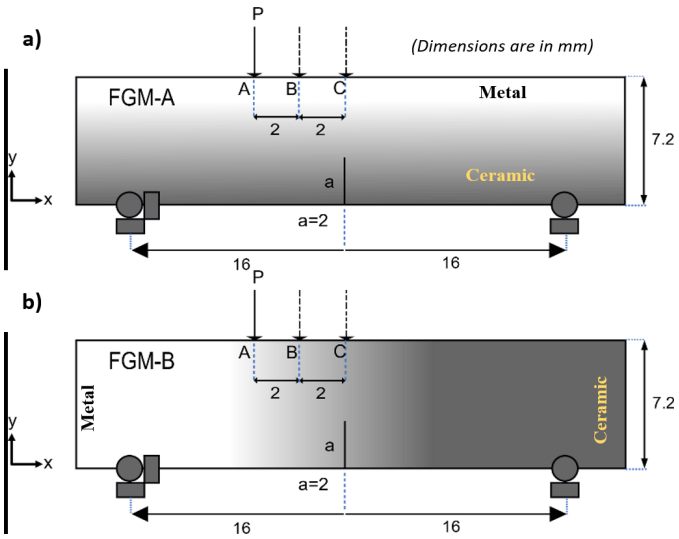

Fig. 4. Geometry and material gradient direction; a) for FGM-A and b) for FGM-B

For this problem, we considered a cracked FGM specimen under three-point bending. A pre-crack with $a = 2$ mm is considered parallel to the material gradient for FGM-A, and grows forward in the direction of decreasing Young's modulus, and perpendicular to the gradient of the properties for FGM-B.

Eight nodded quadratic elements are used to mesh the considered geometry. To take into account the singularities of the fields in the vicinity of the crack-tip, some modifications were

necessary [40-41]. Singular elements were employed to describe the singularity at the crack-tip. The special quarter point finite elements are used for a better approximation of the field near the crack front. The mid-side node of the element connected to the crack front is shifted to the quarter of the element length (Fig. 5). The determination of fracture parameters is based on the creation of singular elements at the crack tip based on isoparametric finite element developed into the APDL program. This method has proven its effectiveness in previous studies [42-45].

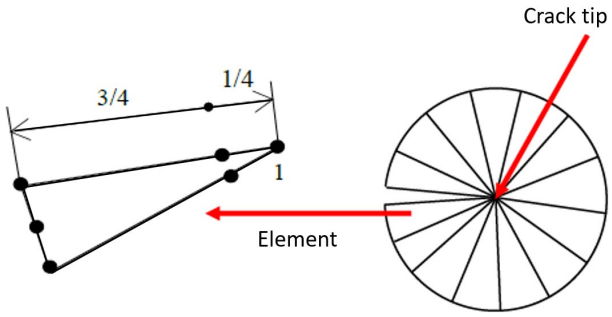

Fig. 5. Singular elements at the crack-tip

The meshing is considered to calculate the T-stress and the SIFs K_I and K_{II} using DCT method to predict the fracture trajectory for every step of crack growth. The calculation of the fracture parameters is performed under plane strain conditions. According to Noda and Jin [46] the influence of Poisson's ratio can be neglected for functionally graded materials, thus Poisson's ratio is considered $\nu = 0.3$ for the whole model.

Fig. 6 shows the geometrical model of FGM beam and expose the *FE* mesh of the specimen subjected to bending with a zoom on the crack front mesh. Fig. 7 presents the elastic modulus E gradient for the FGM-A and FGM-B. The mechanical properties E, ν and K_{IC} (fracture toughness) were taken from the experiments of Xin Jin et al. [28]. The detailed values of the material gradation are summarized TABLE 1 for each layer of the FGM.

TABLE 1

Material properties for each layer of the considered FGM

Material composition Ceramic/Metal	E (GPa)	K_{IC} (MPa.$\sqrt{m}$)
100/0	201	11
90/10	188	9.4
80/20	170	7.5
70/30	152	6.2
60/40	135	4.7
50/50	120	3.8

5. Results and discussion

Figs. 8, 9 and 10 illustrate respectively the variation of the mixed mode SIFs K_I and K_{II} as well as the T-stress in the case of FGM-A and FGM-B. The value of K_I increases during crack

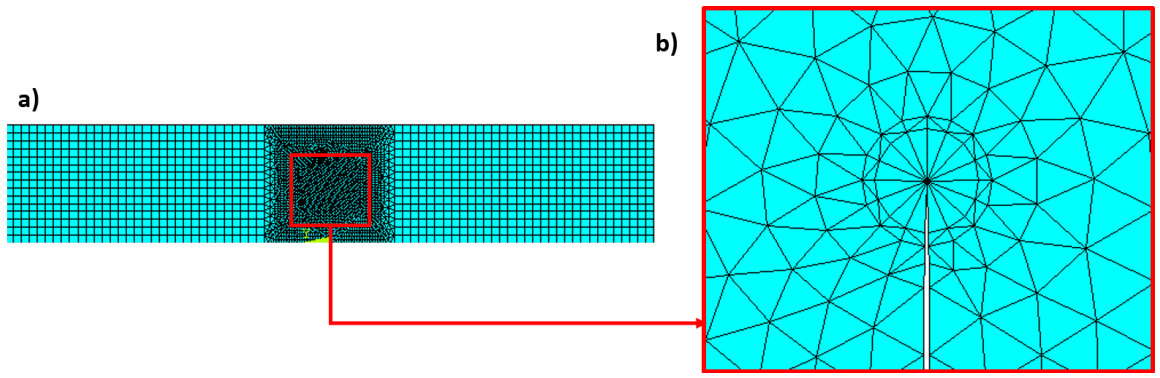

Fig. 6. FE mesh and zoom on crack-tip

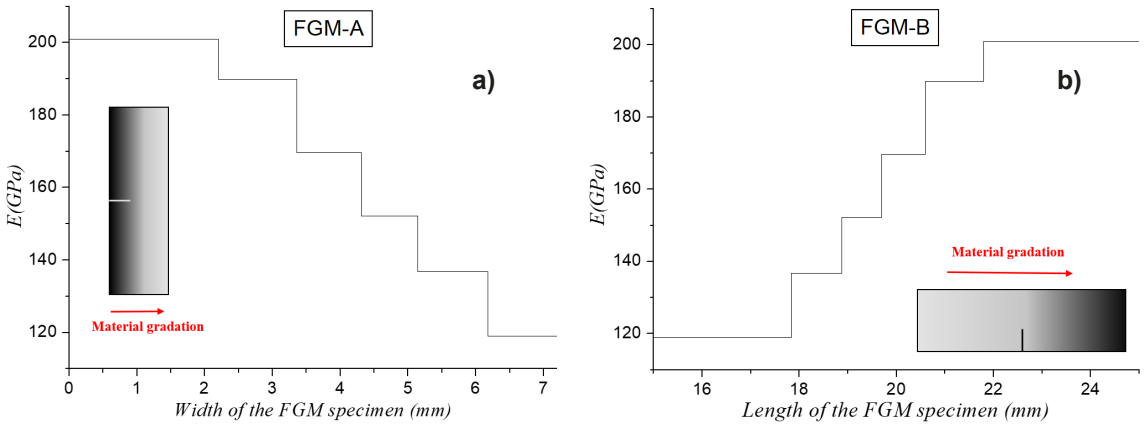

Fig. 7. Elastic modulus variation of the considered materials [28]: a) FGM-A and b) FGM-B

extension. In all cases, K_I has a major effect on the driving force of the crack propagation. However, K_{II} defines the deviation from the stable mode I crack propagation and tends to oscillate around zero during the propagation.

The evolution of the normalized T-stress is presented in the Fig. 10, its magnitude is smaller compared to that of K_I in the first part of the crack propagation, and then it takes significant values in the last stages. We note a negative magnitude in the early stages of propagation for both FGM-A and FGM-B materials, then T-stress changes sign to positive. This could be an indication of the instability of the crack propagation.

Using the MTS criterion, we have plotted in Fig. 11 the crack propagation trajectories corresponding to the two materials FGM-A and FGM-B for the three loading positions (A, B and C). In the case of loading in positions A and B, the crack propagation trajectory leans toward left in the direction of the loading point, which creates a mixed mode conditions. This is noticed for both materials, however, for the FGM-B, the crack takes a more curved trajectory followed by an increasing of the bifurcation angle as the crack continue to grow.

For a better illustration of this phenomenon, we can focus on the comparison presented in Fig. 11c for the loading position C. In this case, the condition is in mode I, the crack is supposed to propagate in a straight direction with respect to the initial crack, which is the case for FGM-A. However, in the case of FGM-B, the propagation trajectory deviates from the initial direction. Due to the identical geometry and boundary conditions of the FGM beams, this can be explained by the type of the FGM-B

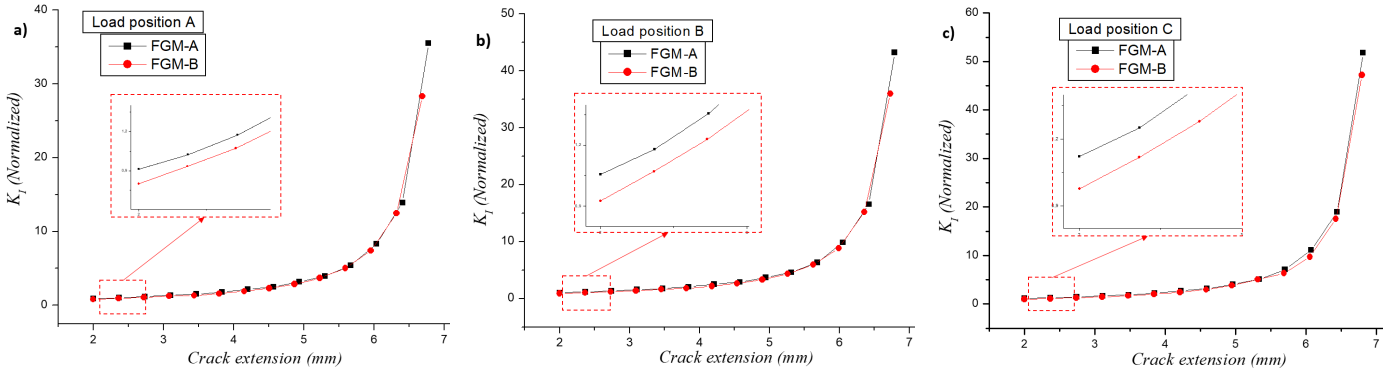

Fig. 8. Evolution of the normalized mode I SIF for FGM-A and FGM-B as a function of crack extension at loading positions; a) A, b) B, c) C

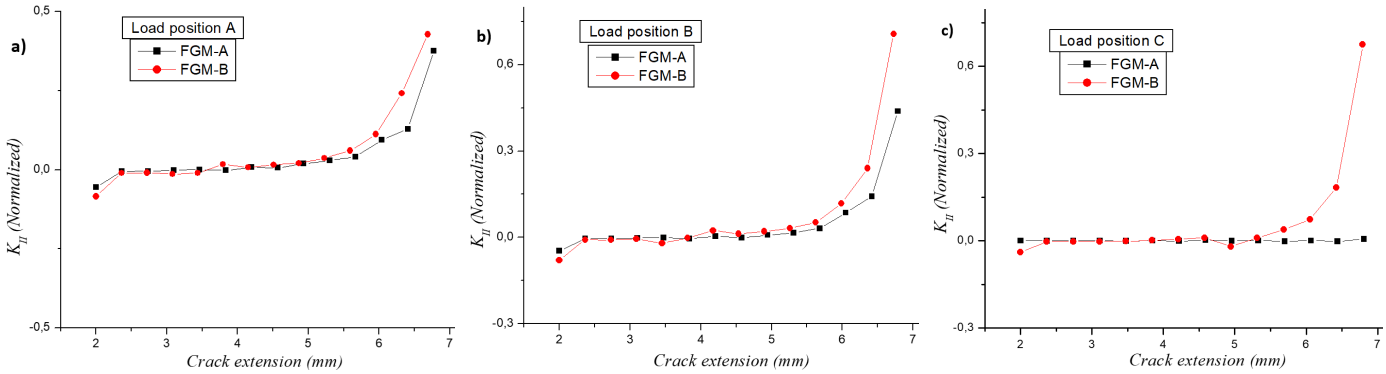

Fig. 9. Evolution of the normalized mode II SIF for FGM-A and FGM-B as a function of crack extension at loading positions; a) A, b) B, c) C

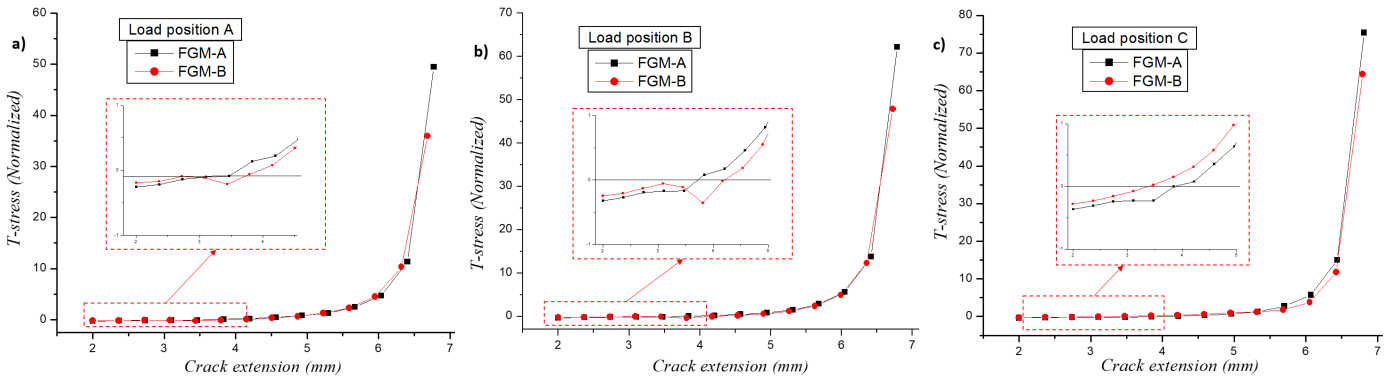

Fig. 10. Evolution of the normalized T-stress for FGM-A and FGM-B as a function of crack extension at loading positions; a) A, b) B, c) C

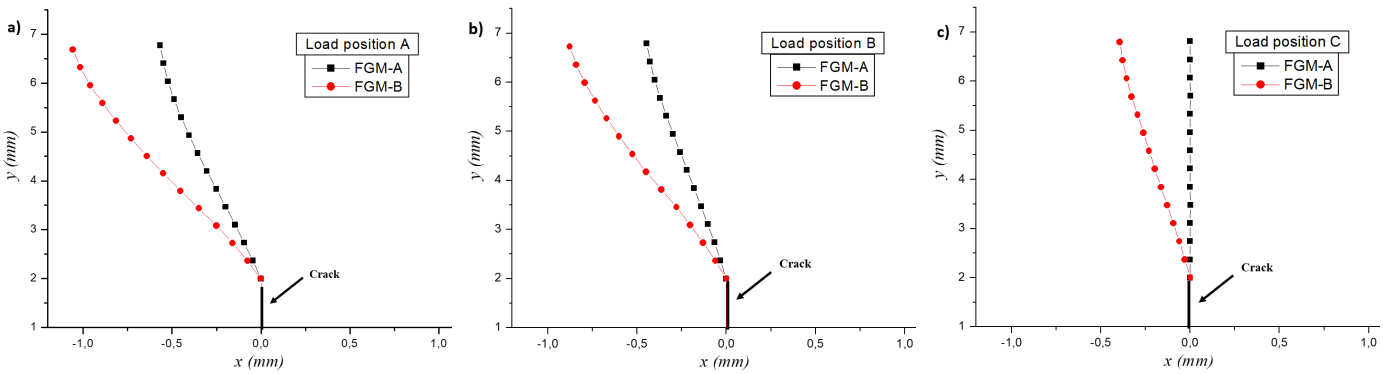

Fig. 11. Numerical predictions of the crack growth trajectories of FGM-A and FGM-B at different loading positions; a) A, b) B, c) C

material where the gradation direction is perpendicular to the direction of the initial crack, which means that the value of the elastic modulus decreases in this direction and the crack takes the easiest trajectory to propagate.

Without a doubt, the material gradient has a considerable effect on the crack trajectory in FGMs. Moreover, it can be concluded that the easiest way for the crack propagation is when the crack is perpendicular to the material gradation where the crack deviates towards the side of the decreasing properties.

A comparison between the kinking angles θ_0 of both materials is presented in TABLE 2. It is noted that for FGM-A, the crack bifurcation takes place at an initial angle of 6.97° with respect to the crack axis. While, the kinking angle for FGM-B is 11.82°. From the numerical results, one can conclude that the crack located on the rigid side of the FGM beam kinks less than the one on the soft side.

TABLE 2

Predicted fracture initial angles for FGM-A and FGM-B

Load position	Kinking angle θ_0	
	FGM-A	FGM-B
A	6,97	11,82
B	4,98	9,63
C	0,0185	4,56

Based on the fracture criterion, the critical load is determined for every crack extension, and the obtained value is applied to the corresponding extension. Fig. 12 shows that the critical load required to the crack growth for FGM-A is greater

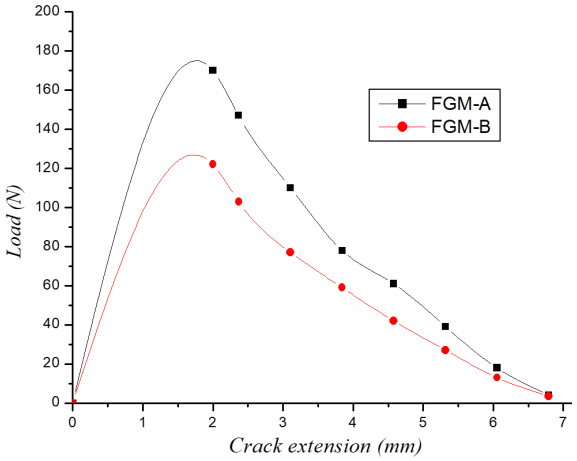

Fig. 12. Comparison of the critical load as a function of crack extension for FGM-A and FGM-B

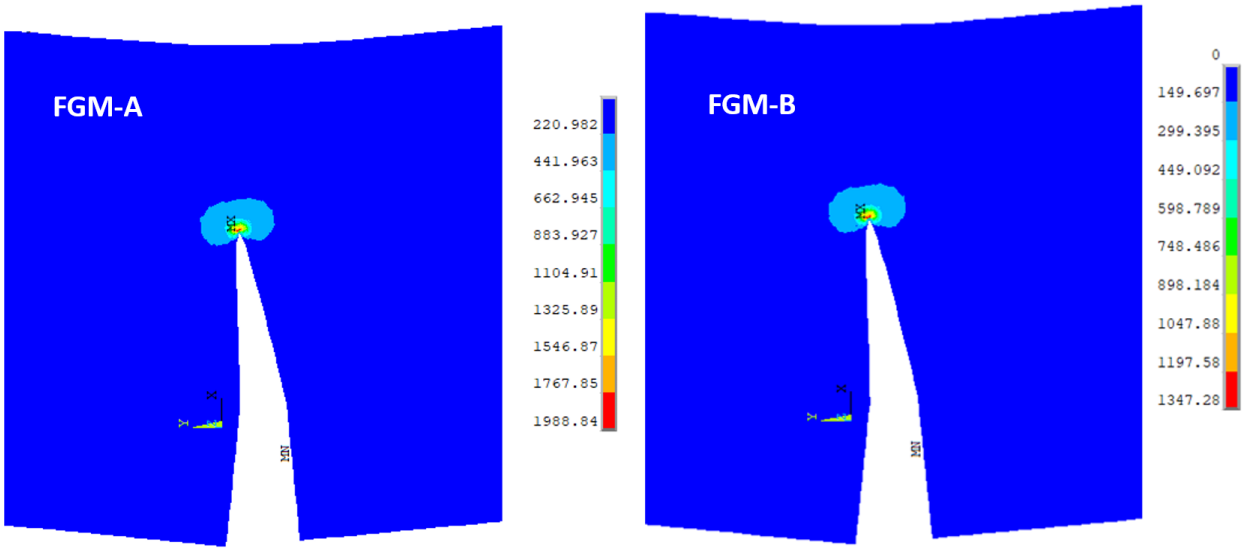

Fig. 13. Stress distribution maps of FGM-A and FGM-B

than that for FGM-B. It depends on the properties of the material, especially the critical stress intensity factor K_{IC}, which corresponds the material resistance to the crack propagation. A crack located in the stiff part of the beam requires a larger load to grow. This is illustrated in Fig. 13 where the stress distribution maps of the studied cases are presented. It is clearly shown that the stresses are more important for the FGM-A than the FGM-B for the same geometry and boundary conditions.

6. Conclusion

The main focus of this numerical study is to explore the effect of the material gradation direction on the fracture trajectory of ceramic/metal FGM beams subjected to mixed-mode loading. Two sorts of functionally graded materials are examined; the FGM-A represents the beam with a parallel pre-crack to the material gradient, and FGM-B with a perpendicular pre-crack to the material gradation. The main findings are highlighted:

– The mode I SIF K_I has a major effect on the driving force of the crack propagation, however K_{II} defines the deviation from the stable crack propagation.
– The change of sign of T-stress could be an indication of the instability of the crack propagation.
– The crack in the FGM-B, follows a more curved trajectory and the crack propagation angle increases as the crack grows.
– The difference of the fracture trajectory can be related to the influence of the material gradation.
– The numerical results of the kinking angle θ_0 demonstrate that the crack located in the rigid part of the specimen exhibits less deviation than the one on the soft part.
– The critical load required to the crack growth for FGM-A is greater than that for FGM-B. It depends on the value of critical stress intensity factor K_{IC}.

REFERENCES

[1] A. Oral, J. Lambros, G.J. Anlas, J. of Applied Mechanics **75** (5) (2008). DOI: https://doi.org/10.1115/1.2936238

[2] Z.J. Zhang, G.H. Paulino, Int. J. of Plasticity **21** (6), 1195-1254 (2005). DOI: https://doi.org/10.1016/j.ijplas.2004.06.009

[3] R. Dimitri, N. Fantuzzi, Y. Li, F. Tornabene, Composite Structures **160**, 468-490 (2017). DOI: https://doi.org/10.1016/j.compstruct.2016.10.067

[4] J.E. Dolbow, M. Gosz, Int. J. of Solids and Struc. **39** (9), 2557-2574 (2002). DOI: https://doi.org/10.1016/S0020-7683(02)00114-2

[5] M.S. Kirugulige, H.V. Tippur, Experimental Mechanics **46** (2), 269-281 (2006). DOI: https://doi.org/10.1007/s11340-006-5863-4

[6] Z.H. Jin, R.C. Batra, J. of the Mech. and Physics of Solids **44** (8), 1221-1235 (1996). DOI: https://doi.org/10.1016/0022-5096(96)00041-5

[7] P. Gu, R.J. Asaro, Int. J. of Solids and Struc. **34** (24), 3085-3098 (1997). DOI: https://doi.org/10.1016/S0020-7683(96)00175-8

[8] M.A. Bouchelarm, M. Mazari, N. Benseddiq, J. of Failure Analysis and Prevention **17** (5), 919-934 (2017). DOI: https://doi.org/10.1007/s11668-017-0322-3

[9] K.K. Choi, J.U. Cho, Arch. Metall. Mater. **62** (2), 1363-1366 (2017). DOI: https://doi.org/10.1515/amm-2017-0209

[10] O.-H. Kim, Y.C. Kim, Arch. Metall. Mater. **60** (2B), 1441-1444 (2015). DOI: https://doi.org/10.1515/amm-2015-0149

[11] K. Yakoubi, S. Montassir, H. Moustabchir, A. Elkhalfi, C.I. Pruncu, J. Arbaoui, M.U. Farooq, Mathematics **9** (5), 507 (2021). DOI: https://doi.org/10.3390/math9050507

[12] S. Montassir, H. Moustabchir, A. Elkhalfi, M.L. Scutaru, S. Vlase, Mathematics **9** (23), 2990 (2021). DOI: https://doi.org/10.3390/math9232990

[13] J. Zych, J. Piekło, M. Maj, A. Garbacz-Klempka, M. Piękoś, Arch. Metall. Mater. **64** (2) 765-771 (2019). DOI: https://doi.org/10.24425/amm.2019.127611

[14] J.H. Kim, G.H. Paulino, Mechanics and Materials in Design **1** (1), 63-94 (2004). DOI: https://doi.org/10.1023/B:MAMD.0000035457.78797.c5

[15] J.H. Kim, G.H. Paulino, Int. J. for Numerical Methods in Eng. **53** (8), 1903-1935 (2002). DOI: https://doi.org/10.1002/nme.364

[16] J.H. Kim, G.H. Paulino, Mechanics of Advanced Materials and Structures **14** (4), 227-244 (2007). DOI: https://doi.org/10.1080/15376490600790221

[17] S. Topal, S. Dag, Mathematical Problems in Engineering **2013** (2013). DOI: https://doi.org/10.1155/2013/315176

[18] N. Benamara, A. Boulenouar, M. Aminallah, Periodica Polytechnica Mechanical Engineering **61** (1), 60-67 (2017). DOI: https://doi.org/10.3311/PPme.9682

[19] M. Chafi, A. Boulenouar, Materials Research **22** (2019). DOI: https://doi.org/10.1590/1980-5373-MR-2018-0701

[20] N. Benamara, A. Boulenouar, M. Aminallah, N. Benseddiq, Structural engineering and mechanics: An international Journal **61** (3), 371-379 (2017). DOI: https://doi.org/10.12989/sem.2017.61.3.371

[21] B.N. Rao, S. Rahman, Engineering Fracture Mechanics **70** (1), 1-27 (2003). DOI: https://doi.org/10.1016/s0013-7944(02)00038-3

[22] K.S.R. Chandran, I. Barsoum, Int. J. of Fract. **121**, 183-203 (2003). DOI: https://doi.org/10.1023/B:FRAC.0000005346.83147.b2

[23] M. Dorduncu, I. Olmus, T. Rabczuk, Comp. Struct. **279**, 114743 (2022). DOI: https://doi.org/10.1016/j.compstruct.2021.114743

[24] D. He, D. Huang, D. Jiang, Theor. App. Fract. Mech. **111**, 102852 (2021). DOI: https://doi.org/10.1016/j.tafmec.2020.102852

[25] K.D. Nguyen, C.L. Thanh, H. Nguyen-Xuan, M. Abdel-Wahab, Engineering with Computers 1-21 (2021). DOI: https://doi.org/10.1007/s00366-021-01518-0

[26] C.E. Rousseau, H.V. Tippur, Acta Materialia **48** (16), 4021-4033 (2000). DOI: https://doi.org/10.1016/S1359-6454(00)00202-0

[27] M.T. Tilbrook, R.J. Moon, M. Hoffman, Eng. Fract. Mechanics **72**, 2444-2467 (2005). DOI: https://doi.org/10.1016/j.engfracmech.2005.04.001

[28] X. Jin, L. Wu, L. Guo, H. Yu, Y. Sun, Eng. Fract. Mechanics **76** (12), 1800-1810 (2009). DOI: https://doi.org/10.1016/j.engfracmech.2009.04.003

[29] J. Abanto-Bueno J. Lambros, Int. J. Solids Struct. **43** (13), 3920-3939. DOI: https://doi.org/10.1016/j.ijsolstr.2005.05.025

[30] J. Abanto-Bueno, J. Lambros, J. Experimental Mechanics **46** (2), 179-196 (2006). DOI: https://doi.org/10.1007/s11340-006-6416-6

[31] B. Sabuncuoglu, S. Dag, B. Yildirim, Computational Materials Science **52** (1), 246-252 (2012). DOI: https://doi.org/10.1016/j.commatsci.2011.06.010

[32] M.L.Williams, J. Appl. Mech. **24**, 109-114 (1957). DOI: https://doi.org/10.1115/1.4011454

[33] M.H. Meliani, Z. Azari, G. Pluvinage, Y.G. Matvienko, Eng. Fract. Mechanics **77** (11), 1682-1692 (2010). DOI: https://doi.org/10.1016/j.engfracmech.2010.03.010

[34] M.H. Meliani, Z. Azari, M. Al-Qadhi, N. Merah, G. Pluvinage, Composites Part B: Engineering **80**, 126-133 (2015). DOI: https://doi.org/10.1016/j.compositesb.2015.05.034

[35] M.R. Ayatollahi, M.J. Pavier, D.J. Smith, Int. J. of Fract. **91** (3), 283-298(1998). DOI: https://doi.org/10.1023/A:1007581125618

[36] F. Erdogan, G.C. Sih, Journal of Basic Engineering **85** (4) 519-525 (1963). DOI: https://doi.org/10.1115/1.3656897

[37] P. Bocca, A. Carpinteri, S. Valente, Int. J. of Solids and Struc. **27** (9), 1139-1153 (1991). DOI: https://doi.org/10.1016/0020-7683(91)90115-V

[38] H. Khazal N.A. Saleh, Mech. Adv. Mater. Struct. **26** (11) 975-983 (2018). DOI: https://doi.org/10.1080/15376494.2018.1432786

[39] X. Chen, T. Luo, E.T. Ooi, E.H. Ooi, C. Song, Theo. App. Fract. Mech. **94**, 120-133 (2018). DOI: https://doi.org/10.1016/j.tafmec.2018.01.008

[40] R.D. Henshell, K.G. Shaw, Int. J. for Num. Meth. in Eng. **9**, 495-507 (1975). DOI: https://doi.org/10.1002/nme.1620090302

[41] R.S. Barsoum, Int. J. for Num. Meth. in Engng. **10**, 25-37 (1976). DOI: https://doi.org/10.1002/nme.1620100103

[42] A. Boulenouar, M.A. Bouchelarm, M. Chafi, J. Interact. Des. Manuf. **18** (2), 649-658 (2024). DOI: https://doi.org/10.1007/s12008-023-01726-6

[43] A. Boulenouar, M.A. Bouchelarm, N. Benseddiq, Steel Compos. Struct. **49** (3), 271-280 (2023). DOI: https://doi.org/10.12989/scs.2023.49.3.271

[44] A. Boulenouar, I. Hebbar, M.A. Bouchelarm, Theor. App. Fract. Mech. **125**, 103886 (2023). DOI: https://doi.org/10.1016/j.tafmec.2023.103886

[45] M. Chafi, M.A. Bouchelarm, A. Boulenouar, N. Benseddiq, Mech. Solids. **58** (6), 2364-2381 (2023). DOI: https://doi.org/10.3103/S0025654423601441